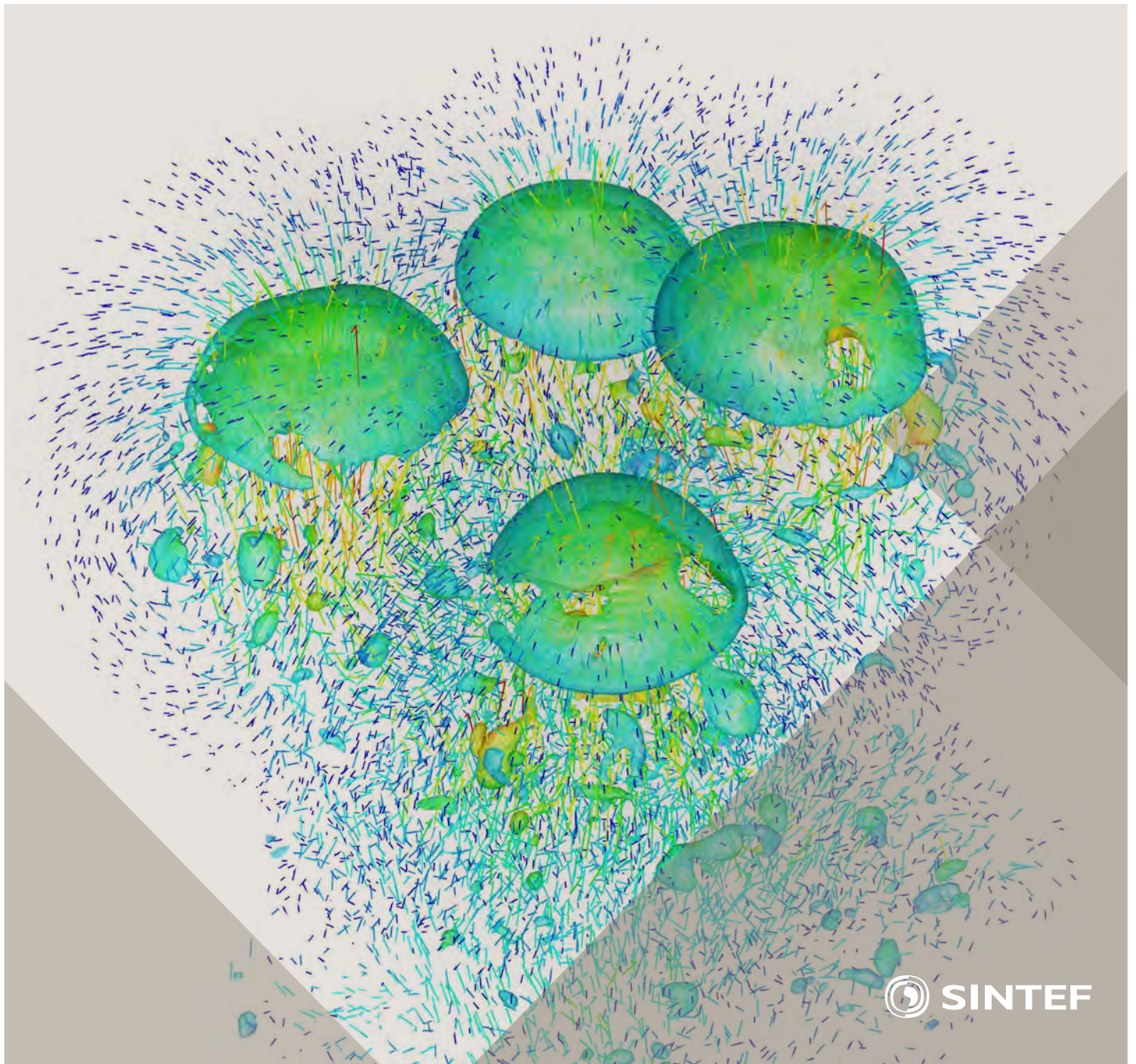


Selected papers from 10th International Conference on
Computational Fluid Dynamics in the Oil & Gas, Metal-
lurgical and Process Industries

Progress in Applied CFD



SINTEF Proceedings

Editors:

Jan Erik Olsen and Stein Tore Johansen

Progress in Applied CFD

Selected papers from 10th International Conference on Computational Fluid
Dynamics in the Oil & Gas, Metallurgical and Process Industries

SINTEF Academic Press

SINTEF Proceedings no 1

Editors: Jan Erik Olsen and Stein Tore Johansen

Progress in Applied CFD

Selected papers from 10th International Conference on Computational Fluid Dynamics in the Oil & Gas, Metallurgical and Process Industries

Key words:

CFD, Flow, Modelling

Cover, illustration: Rising bubbles by Schalk Cloete

ISSN 2387-4287 (printed)

ISSN 2387-4295 (online)

ISBN 978-82-536-1432-8 (printed)

ISBN 978-82-536-1433-5 (pdf)

60 copies printed by AIT AS e-dit

Content: 100 g munken polar

Cover: 240 g trucard

© Copyright SINTEF Academic Press 2015

The material in this publication is covered by the provisions of the Norwegian Copyright Act. Without any special agreement with SINTEF Academic Press, any copying and making available of the material is only allowed to the extent that this is permitted by law or allowed through an agreement with Kopinor, the Reproduction Rights Organisation for Norway. Any use contrary to legislation or an agreement may lead to a liability for damages and confiscation, and may be punished by fines or imprisonment

SINTEF Academic Press

Address: Forskningsveien 3 B
 PO Box 124 Blindern
 N-0314 OSLO

Tel: +47 22 96 55 55

Fax: +47 22 96 55 08

www.sintef.no/byggforsk

www.sintefbok.no

SINTEF Proceedings

SINTEF Proceedings is a serial publication for peer-reviewed conference proceedings on a variety of scientific topics.

The processes of peer-reviewing of papers published in SINTEF Proceedings are administered by the conference organizers and proceedings editors. Detailed procedures will vary according to custom and practice in each scientific community.

PREFACE

This book contains selected papers from the 10th International Conference on Computational Fluid Dynamics in the Oil & Gas, Metallurgical and Process Industries. The conference was hosted by SINTEF in Trondheim in June 2014 and is also known as CFD2014 for short. The conference series was initiated by CSIRO and Phil Schwarz in 1997. So far the conference has been alternating between CSIRO in Melbourne and SINTEF in Trondheim. The conferences focus on the application of CFD in the oil and gas industries, metal production, mineral processing, power generation, chemicals and other process industries. The papers in the conference proceedings and this book demonstrate the current progress in applied CFD.

The conference papers undergo a review process involving two experts. Only papers accepted by the reviewers are presented in the conference proceedings. More than 100 papers were presented at the conference. Of these papers, 27 were chosen for this book and reviewed once more before being approved. These are well received papers fitting the scope of the book which has a slightly more focused scope than the conference. As many other good papers were presented at the conference, the interested reader is also encouraged to study the proceedings of the conference.

The organizing committee would like to thank everyone who has helped with paper review, those who promoted the conference and all authors who have submitted scientific contributions. We are also grateful for the support from the conference sponsors: FACE (the multiphase flow assurance centre), Total, ANSYS, CD-Adapco, Ascomp, Statoil and Elkem.

Stein Tore Johansen & Jan Erik Olsen



Organizing committee:

Conference chairman: Prof. Stein Tore Johansen
Conference coordinator: Dr. Jan Erik Olsen
Dr. Kristian Etienne Einarsrud
Dr. Shahriar Amini
Dr. Ernst Meese
Dr. Paal Skjetne
Dr. Martin Larsson
Dr. Peter Witt, CSIRO

Scientific committee:

J.A.M. Kuipers, TU Eindhoven
Olivier Simonin, IMFT/INP Toulouse
Akio Tomiyama, Kobe University
Sanjoy Banerjee, City College of New York
Phil Schwarz, CSIRO
Harald Laux, Osram
Josip Zoric, SINTEF
Jos Derksen, University of Aberdeen
Dieter Bothe, TU Darmstadt
Dmitry Eskin, Schlumberger
Djamel Lakehal, ASCOMP
Pär Jonsson, KTH
Ruben Shulkes, Statoil
Chris Thompson, Cranfield University
Jinghai Li, Chinese Academy of Science
Stefan Pirker, Johannes Kepler Univ.
Bernhard Müller, NTNU
Stein Tore Johansen, SINTEF
Markus Braun, ANSYS

CONTENTS

Chapter 1: Pragmatic Industrial Modelling	7
On pragmatism in industrial modeling	9
Pragmatic CFD modelling approaches to complex multiphase processes.....	25
A six chemical species CFD model of alumina reduction in a Hall-Héroult cell	39
Multi-scale process models to enable the embedding of CFD derived functions: Curtain drag in flighted rotary dryers	47
Chapter 2: Bubbles and Droplets	57
An enhanced front tracking method featuring volume conservative remeshing and mass transfer	59
Drop breakup modelling in turbulent flows	73
A Baseline model for monodisperse bubbly flows	83
Chapter 3: Fluidized Beds	93
Comparing Euler-Euler and Euler-Lagrange based modelling approaches for gas-particle flows.....	95
State of the art in mapping schemes for dilute and dense Euler-Lagrange simulations	103
The parametric sensitivity of fluidized bed reactor simulations carried out in different flow regimes.....	113
Hydrodynamic investigation into a novel IC-CLC reactor concept for power production with integrated CO ₂ capture	123
Chapter 4: Packed Beds	131
A multi-scale model for oxygen carrier selection and reactor design applied to packed bed chemical looping combustion	133
CFD simulations of flow in random packed beds of spheres and cylinders: analysis of the velocity field	143
Numerical model for flow in rocks composed of materials of different permeability.....	149
Chapter 5: Metallurgical Applications	157
Modelling argon injection in continuous casting of steel by the DPM+VOF technique.....	159
Modelling thermal effects in the molten iron bath of the HIs melt reduction vessel.....	169
Modelling of the Ferrosilicon furnace: effect of boundary conditions and burst	179
Multi-scale modeling of hydrocarbon injection into the blast furnace raceway.....	189
Prediction of mass transfer between liquid steel and slag at continuous casting mold	197
Chapter 6: Oil & Gas Applications	205
CFD modeling of oil-water separation efficiency in three-phase separators.....	207
Governing physics of shallow and deep subsea gas release	217
Cool down simulations of subsea equipment.....	223
Lattice Boltzmann simulations applied to understanding the stability of multiphase interfaces.....	231
Chapter 7: Pipeflow	239
CFD modelling of gas entrainment at a propagating slug front.....	241
CFD simulations of the two-phase flow of different mixtures in a closed system flow wheel.....	251
Modelling of particle transport and bed-formation in pipelines	259
Simulation of two-phase viscous oil flow	267

A MULTI-SCALE MODEL FOR REACTOR DESIGN AND OXYGEN CARRIER SELECTION APPLIED TO PACKED BED CHEMICAL LOOPING COMBUSTION

Mandar TABIB¹, John MORUD², Stein Tore JOHANSEN¹, Shahriar AMINI^{1*}

¹ Flow Technology Department, SINTEF Materials and Chemistry, Trondheim, Norway.

² Chemical Engineering Department, SINTEF Materials and Chemistry, Trondheim, Norway

* E-mail: Shahriar.Amini@sintef.no

ABSTRACT

Proper selection of a catalyst shape (or a particle shape) can improve the performance of a gas-solid packed bed reactor. The particle shape affects the packing structure and the transport phenomena within the packed bed. This information is not available for many non-spherical particle shapes which limit reactor design options. To enable catalyst and reactor design, a validated 3D Computational Fluid Dynamics (CFD)-Discrete Element Method (DEM) model has been developed to resolve the flow around these particles and to obtain information on the transport phenomena (pressure drop correlation and heat/mass transfer coefficient). The DEM is used to obtain realistic packing structures for different particle shapes, and the CFD is conducted on these DEM generated packing structure. However, the 3D CFD-DEM model cannot be applied on the whole reactor as it is computationally prohibitive. Hence, a multi-scale modelling approach is developed, wherein correlations obtained by the 3D CFD-DEM model from a representative 3D volume of the packed bed are used as closures in a 1D model for reactor design. The validations for all the models have been done. The multi-domain 1D particle-reactor model developed here is a combination of (1) a particle model for radial distribution of chemical species and temperature within a catalyst particle and (2) a 1D reactor model for mass and energy balance along the reactor. This 1D model is able to account for both intra-particle and inter-particle heat and mass transfer phenomena. The proposed multi-scale modelling approach has been applied to select an appropriate oxygen carrier shape for a Chemical Looping Combustion (CLC) packed bed reactor. This work compares the performance of different oxygen carrier shapes (fluted ring shape, cylindrical pellet shape and spherical shape) in terms of reactor operation. The simulations are used to recommend a pellet shape that offers least pressure drop, highest conversion and no early fuel slip for efficient CO₂ capture.

Keywords: Chemical looping combustion, Catalyst design, Packed bed reactor, Multi-scale modelling, CO₂ capture, Discrete Element Modelling, CFD.

NOMENCLATURE

Latin

A	Blake–Kozeny–Carman constant	[]
a	Particle surface area per volume of bed	[m ² /m ³]
B	Burke-Plummer constant	[]
C	Concentration	[kmol/m ³]
C _p	Heat capacity	[J/kg.K]
D _{eff}	Effective diffusivity	[m ² /s]
d _p	Particle diameter	[m]
F _h	Flux of enthalpy	[J/m ² .s]
F	Flux	kmol/m ² .s

G	Mass flux of gas	[kg/m ² .s]
h	Heat transfer coefficient	[W/m ² .K]
H	Enthalpy	[J/kmol]
k _g	Mass transfer coefficient	[m/s]
M	Molecular Weight	[Kg/kmol]
P	Pressure	[bar]
R	Particle radius	[m]
R _g	Gas constant	[J/kmol.K]
T	Temperature	[K]
t	Time	[s]
U	Internal energy	[J/m ³]
X _k	Mass fraction of species "k"	[-]
X _j	Conversion of species j	[-]
v _g	Superficial gas velocity	[m/s]
w _f	Fluid mass flow rate	[Kg/s]
w	Weight fraction	[-]
z	Axial position	[m]
r	radial position	[m]
c _∞	Concentration in bulk phase	
r _l	Reaction rate of species "l"	[kmol/Kgs]

Greek

-ΔH _{rx}	Heat of reaction	[J/kmol]
ε	Void fraction	[-]
ξ	Ratio of moles of gas to solid needed for the reaction	
Γ _k	Source term for species "k"	[kmol/m3.s]
Γ _u	Source term for enthalpy	[J/m3.s]
λ	Particle thermal conductivity	[W/m.K]
λ _{ax}	Effective bed thermal conductivity	[W/m.K]
μ	Gas viscosity	[kg/m.s]
ρ	Gas density	[kg/m3]
ρ _s	Oxygen carrier density	[kg/m3]
τ	Oxygen carrier tortuosity	[-]

Sub/superscripts

k	Species "k"
tot	Total
g	Gas phase
s	Solid particle
l	Number of Reactions
kg	Gas species in gas phase
ks	Gas species in particle pores
j	Active solid species j

INTRODUCTION

Significant performance improvements can be obtained in a packed bed reactor by understanding the role of the particle in influencing the intra-particle and inter-particle transport phenomena. The particle can be a catalyst or an oxygen carrier (as in CLC based applications). The physical feature of a particle influences the overall packing structure, pressure drop, heat-transfer, mass-transfer and overall reaction rate in the reactor. Hence, researchers experimentally study different particle shapes (spheres, cylinder, fluted rings, tri-lobe, quadrulobe, monoliths, wagon wheels, hollow extrudates, discs, etc) to identify the most suitable shape/size for a given process. Selecting a suitable particle shape and size involves making compromises between reactivity and pressure drop.

In this regard, development of an accurate modelling approach for enabling catalyst (pellet) shape selection and reactor design will be useful. The packed-bed reactor offers an ideal platform to develop a multi-scale model that can account for the multi-scale phenomena in the packed bed, like: (a) at the pore level within the particle, the reactant gas species diffuses and reacts at the internal pore surface. For processes with high intrapellet Damkohler number (like, for the CLC process under study, it is two orders of magnitude high), the diffusional resistances will play an important role as the species diffusivity is low and intrinsic rate kinetics is fast, (b) at the microscopic boundary layer level formed at external surface of the particles may offer viscous resistance to the flow, and offer external resistance to the transport of gaseous species and heat from bulk gas phase to the particle surface, (c) at the meso-scale (interstitial regions between particles): the wakes behind the particles results in additional form drag and will influence the heat and mass transfer, (d) at the reactor level, the movement of thermal and reaction fronts in the entire bed needs to be captured. The influence of reactor geometry on packing structure and the near wall effects (which is dependent on ratio of particle diameter to reactor diameter) needs to be accounted.

These multi-scale effects can be resolved by accounting and simulating the actual particles in a 3D simulation. But, simulating the whole reactor with particles is prohibitive owing to high mesh grid requirements and computational time. Few multi-scale models have been proposed in literature to overcome this difficulty. Ingram (2004) has showed how three different multi-scale strategies (Multi-domain, Parallel and Embedded) can be applied to simulate a packed bed reactor. From application point of view, the use of simultaneous multi-scale (CFD only) or Parallel multi-scale approach (CFD+1D) are also prohibitive. Here, we propose a novel multi-scale modelling approach that can enable catalyst shape selection and reactor design in an efficient and effective way using a validated 3D-CFD-DEM modelling tool in-conjunction with a validated multi-domain 1D particle-reactor model. The methodology is explained in the next section.

MULTI-SCALE METHODOLOGY

A multi-domain 1D particle-reactor model is an efficient tool for large industrial-scale reactor design, as

advanced modelling tools like 3D CFD-DEM will be computationally prohibitive to apply on larger scales. However, the 1D model will need accurate closure information to arrive at precise results. The required closure information involves information on packing structure (porosity, particle surface area per unit reactor volume) and information on transport phenomena (pressure drop correlation, external heat transfer and mass transfer correlation). For many non-spherical particles, such closure information is not available.

In the proposed multi-scale methodology, 3D CFD is applied on a representative volume of a DEM generated packed-bed to obtain the closure information for the 1D model. The use of a representative volume makes the simulations computationally tractable. The Discrete Element Method (DEM) is used to generate a realistic packing structure for spherical/non-spherical particles. In an earlier work (Tabib et. al., 2013), a validated 3D CFD-DEM methodology has been developed to select the dimensions (size) of the bed-segment which can serve as a good representative for the whole packed bed. The 1D model uses the accurate closures derived by the 3D CFD-DEM model to design the large-scale reactor and to study the effect of particle shape/size on the reactor performance. Figure 1 illustrates this multi-scale concept. This form of multi-scale modelling can be termed as a 'Serial by Simplification' multi-scale approach.

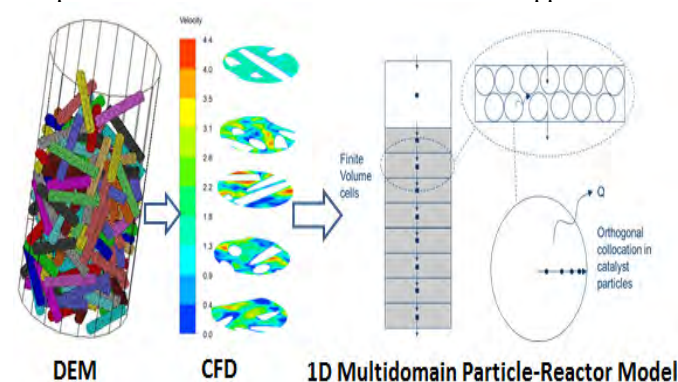


Figure 1 shows schematic representation of Multi-scale formalism. The 3D DEM generates a packed-bed structure, and then 3D CFD is applied on the DEM generated bed-segment to obtain closures for the multi-domain 1D Particle-Reactor model. The 1D model comprises of Finite Volume method on axially discretised reactor space and orthogonal collocation technique on radially discretised particle model.

The devised multi-scale methodology can be described step-wise as:

1. Model the shape of the non-spherical particle using multiple spheres (called multi-sphere approach). For this work, the Fluted ring shape and cylindrical pellet shapes with Aspect ratio 1 (AR1), Aspect ratio 2 (AR2) pellet and Aspect ratio 7 (AR7) pellet have been created. Figure 2 shows the cylindrical pellet (AR7) and the Fluted Ring particle. These shapes are selected to evaluate them for application in a gas-solid non-catalytic Chemical looping combustion unit for power generation integrated with CO₂ capture.
2. Fill a volume (or reactor vessel) with the new catalyst/oxygen carrier shape using Discrete Element

Method. Figure 2 shows the packing structure generated for different particle shapes.

3. Obtain information on bed voidage (or solid porosity profile) and overall particle surface area per unit reactor volume from the DEM generated packing structure. Figure 3 shows the porosity profile obtained for each DEM generated packing and Table 1 shows the particle surface area per unit reactor volume. This information is to be used as closure for the 1D model.

4. Identify the minimum size of the DEM-generated bed-segment that can be a representative of the whole packed bed. The validated methodology to select the cut-segment size is described in Tabib et. al. (2013). The methodology relies on examining the sensitivity of CFD results to varying sample volume size (or to varying dimensions of the cut-segments).

5. The selected cut-segment size is used to simulate flow for wide-range of Reynolds numbers using CFD. Figure 4 shows the 3D CFD-DEM applied on fluted ring and cylindrical pellet. The pressure drop and particle heat transfer coefficient results at different Reynolds number are used to develop an engineering correlation for each of the particle shape.

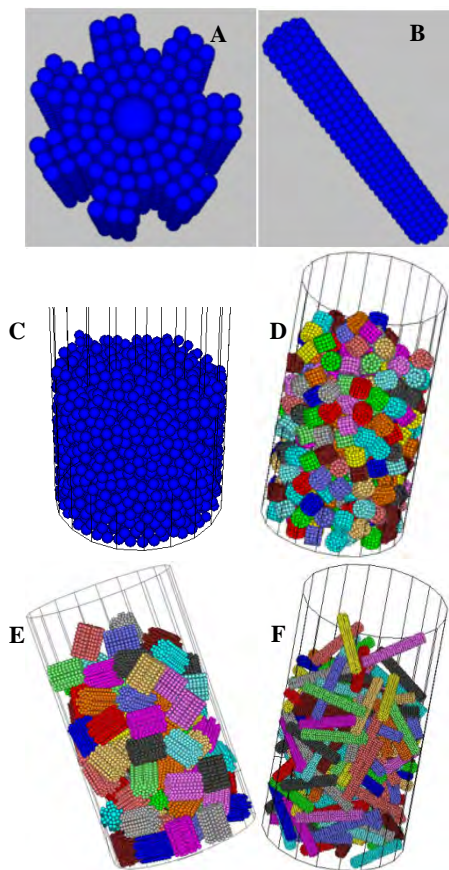


Figure 2 shows (A) Fluted ring particle and (B) cylindrical pellet with aspect ratio 7 generated using multi-sphere approach and the DEM generated packing structure for (C) spherical particle, (D) Aspect ratio 1 particle, (E) Aspect ratio 7 and (F) Fluted Ring.

6. Use the transport phenomena and packing structure information obtained for each packing as closure for the 1D model. The 1D model provides information on

conversion profiles, temperature profiles, fuel slip and pressure drop for large scale industrial reactor.

7. Select the catalyst/oxygen carrier shape that provides the lowest pressure and higher reactivity with no fuel slip, and decide the reactor cycle time.

VALIDATION OF MODELS USED IN MULTI-SCALE METHODOLOGY

The 3D DEM-CFD and 1D model developed to implement the proposed multi-scale approach must be validated. The section covers the validation of 3D DEM-CFD model for predicting accurate closures and the validation of 1D model in accurately simulating a CLC operation.

Validation of DEM generated packing and porosity information

Bed voidage and total particle surface area within a reactor volume are important parameters that affect reactivity, pressure drop and cycle-time. Hence, voidage predicted by DEM has been validated with well-established correlations and with the values reported in literature. Figure 2C-2F shows the DEM generated packing for a spherical packing, two cylindrical pellets packing with pellets of aspect ratio 1 and 7, and a fluted ring packing.

The DEM predicted radial variation of bed-voidage (or porosity) for the spherical packing is similar to that predicted by De Klerk (2003) correlation (as seen in Figure 3). Both predict the voidage oscillations to exist up-to a distance of 5 particle-diameters from the wall (see Figure 3A), after which the oscillations settle down to a constant uniform bulk voidage. The constant bulk voidage (bulk porosity) of DEM generated spherical bed packing is around 0.404, which is same as that predicted by Dixon's correlation (1988) and by De Klerk correlation (2003). The amplitude of oscillations predicted by DEM is lower than the De-Klerk prediction. However, the current 1D model requires the constant bulk voidage as an input and not the radial profile. The bulk voidage predictions in DEM are affected by the particle-particle friction coefficient and particle-wall friction coefficient parameters (value of 0.3 used in this work). If the friction coefficient is high, then the particle will get balanced on each other and counteract the gravity. So, a higher friction coefficient would cause a loose packing (leading to higher porosity). Since, the bulk porosity prediction is accurate, so the current DEM parameters can be considered for further studies. The PFC3D software has been used to conduct these DEM simulations and uses the Hertz-Mindlin model to simulate particle collisions and motion.

Figure 3 shows the radial profiles of voidage (porosity) for the spherical particle (Figure 3A), cylindrical pellets with aspect ratio 1 (Figure 3B), aspect ratio 2 (Figure 3C) and aspect ratio 7 (Figure 3D). DEM predicts that as the aspect ratio of pellet increases (or as the non-sphericity increases), the amplitude and frequency of the near-wall radial bed-voidage oscillations decreases and

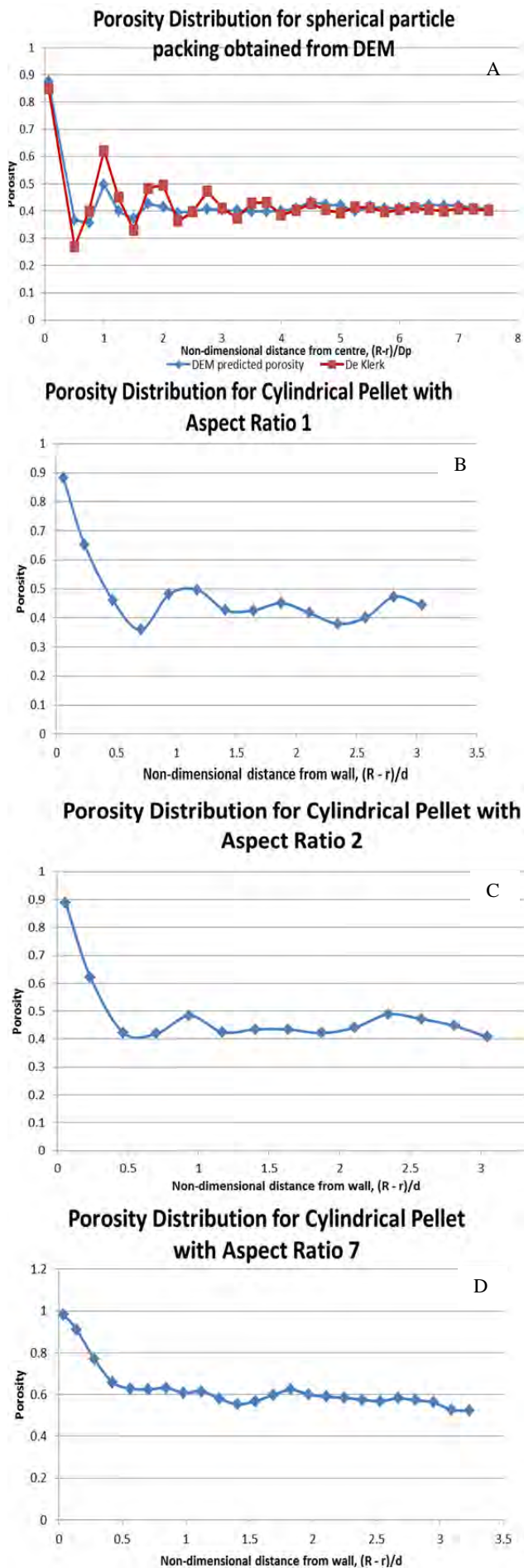


Figure 3 Porosity distribution obtained from DEM generated packing for (A) sphere, (B) AR1, (C) AR2 and (D) AR7.

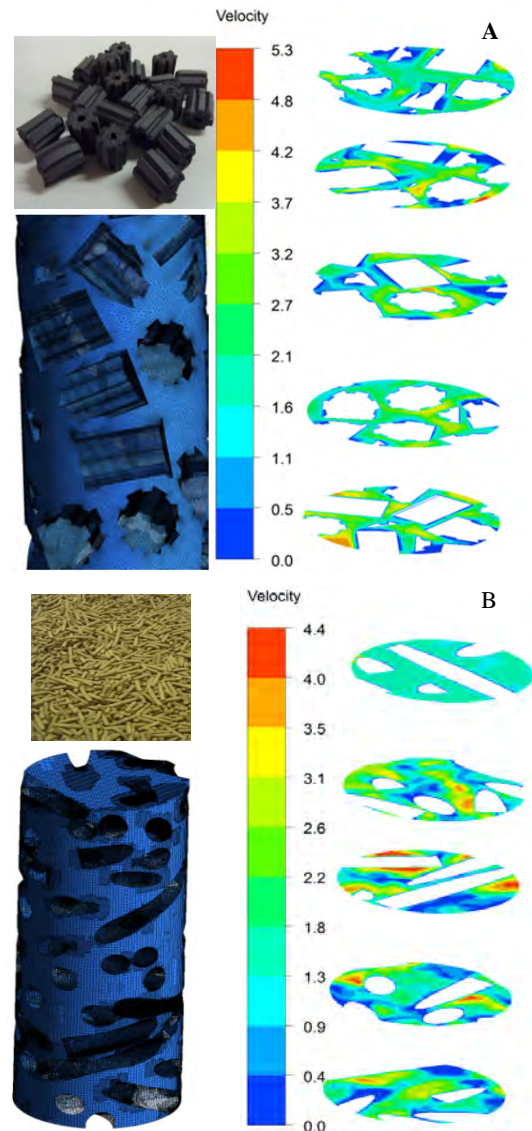


Figure 4 shows 3D CFD-DEM applied on (A) fluted ring and (B) cylindrical pellet.

the wall effect is confined to lesser distance from wall (Figure 3). As seen in Figure 3, there are more oscillations in radial voidage profile for aspect ratio 1 pellet than for aspect ratio 2 pellet. The Aspect ratio 7 pellet shows the least oscillatory behaviour. Comparatively, amongst the three pellets, the radial voidage profile of aspect ratio pellet 1 packing is nearer in behaviour to the spherical packing. The near wall region in Aspect ratio 1 and spherical extends upto five particle-diameters from wall, while for aspect ratio 7 and aspect ratio 2, the near-wall region is limited to two particle diameters from wall. These DEM predictions are quite similar to the observations made by various researchers regarding the variation of bed-voidage with variation of non-sphericity (Roblee (1958), Bey and Eigenberger (1997), Giese et. al. (1998), Caulkin et. al. (2012)). The work done by Nemeč and Levec (2005) suggests that with increasing aspect ratio, the bed voidage increases. DEM is also predicting a higher voidage as the aspect ratio of the pellet increases. Thus, DEM predictions for bulk porosity have been validated with well-established correlations for spherical particle and match the observed trends for non-spherical particles.

Validation of 3D CFD-DEM methodology for obtaining closure information

The validation of CFD-DEM methodology to determine the cut-segment size and to obtain the correlations has been presented in Tabib et. al. (2013). Tabib et. al. (2013) conducted CFD simulations on the DEM generated packing segments for a wide particle Reynolds number range (from laminar to turbulent regime) for both the spherical and non-spherical particles. For the spherical particles, the validation was done by comparing the results with well-established correlations, like: Ergun equation (1952) for pressure drop, Wakao correlation (1979) and multi-particle Ranz-Marshall correlation (1952) for particle heat transfer coefficient and Dixon-Lubua (1985) and Colledge-Paterson (1984) correlation for wall heat transfer coefficient. For the non-spherical particles, the correlations obtained for the long cylindrical pellet (aspect ratio 7) packed bed has been compared with the correlation provided by Nemeec and Levec (2005) for cylindrical pellet with aspect ratio of 5.77. These comparisons had shown good agreements. This validation gave us the confidence that the proposed CFD-DEM methodology can be used for obtaining useful information on transport phenomena within the bed, which can be used for designing and comparison of performance of large-scale packed bed reactor composed of unique particle shapes. The correlations developed for Aspect ratio 7 pellet and Fluted Ring using this methodology has been used in this work. Table 1 cites the input to be provided to 1D model as closure using the results from 3D CFD – DEM approach.

Validation of 1D model for a chemical looping combustion process (gas-solid non-catalytic reactions)

The 1D model is validated with analytical results for a packed-bed chemical looping combustion (CLC) reactor, which involves cyclic gas-solid non-catalytic reactions. The next section describes the 1D model.

1D model

A software application based on a 1D particle-reactor model has been developed to simulate a packed bed reactor operation. The developed 1D particle-reactor model is a combination of (1) a particle model for simulating radial distribution of chemical species and temperature within a catalyst/oxygen carrier particle and (2) a 1D reactor model for solving mass and energy balance along the reactor. The model accounts for the effect of intra-particle and inter-particle heat and mass transfer on the reactor performance. The reactor model and particle model are coupled together using mass and heat source terms computed at the particle surface. The 1D particle-reactor model can simulate for several different particle shapes (cylindrical pellet, slab and sphere) and offers flexibility in choice of closures (pressure drop correlations, heat-transfer/mass-transfer correlations, voidage and total particle surface area per unit reactor volume). The solution methodology involves a Finite Volume discretization technique for solving gas-phase equations along the reactor and an orthogonal collocation technique for solving the reaction-diffusion

equations within the particle. This code is written in Fortran-90, and is easy to use as Microsoft Excel interface has been created. The Fortran-90 code has been compiled into a direct link library (dll) form and is linked to the excel sheet using Visual Basic for Application (VBA) programming language. The coded 1D model solves the following equations. All the variables are explained in notation.

Ideal gas equation of state

$$P = C_{tot} R_g T_g \quad 1$$

Ergun pressure drop equation

$$\frac{\partial P}{\partial z} = -\frac{G}{\rho d_p} \left(\frac{1-\epsilon_g}{\epsilon_g^3} \right) \left(\frac{A(1-\epsilon_g)\mu}{d_p} + BG \right) \quad 2$$

Material balance for species "k" in gas phase

$$\epsilon_g \frac{\partial C_k}{\partial t} + \frac{\partial F_k}{\partial z} = \Gamma_k$$

$$\text{where, } F_k = F_{tot} X_k - C_{tot} D_{eff,k,g} \frac{\partial X_k}{\partial z} \quad 3$$

Energy balance for gas phase

$$\epsilon_g \frac{\partial U}{\partial t} + \frac{\partial F_h}{\partial z} = \Gamma_U$$

$$\text{where, } F_h = F_{tot} H - \lambda_{ax} \frac{\partial T}{\partial z} \quad 4$$

Boundary conditions for gas phase

$z=0$: mass and energy inlet flux

$$z=L: \quad \frac{\partial C_k}{\partial z} = 0, \quad \frac{\partial T}{\partial z} = 0$$

5

Source terms for gas phase mass- and energy balance arising due to mass and heat transfer at the gas-particle interface.

$$\Gamma_k = k_g a (C_{k,r=R}^s - C_k)$$

$$\Gamma_U = h a (T_{r=R}^s - T)$$

6

for computing h , $\frac{hd_p}{k} = 2.0 + A_c Re_p^x Pr^y$

where, the heat transfer coefficient (h) is computed using the Ranz-Marshall equation shown above and k_g is the mass transfer coefficient. The constant A_c for fluted ring and AR7 packed bed system has been obtained by fitting the CFD-DEM heat transfer results to the above Ranz-Marshall correlation (1952) (as described in Tabib. et. al. (2013)).

Solid particle (oxygen carrier or catalyst) model

Mass balance for species "k" inside a catalyst particle volume

$$\epsilon_s \frac{\partial C_k^s}{\partial t} = \frac{\epsilon_s D_{eff,ks}}{\tau} \nabla^2 C_k^s + \rho_s r_k \quad 7$$

Where, ε_s is the porosity in the particle, $m^3_{pore}/m^3_{particle}$ and C_k^s is $Kmol/m^3_{pore}$. $D_{eff,ks}$ is diffusivity of gas species k .

Energy balance for a catalyst particle volume

$$\rho_s C_{ps} \frac{\partial T^s}{\partial t} = \lambda \nabla^2 T^s + \rho_s \sum_l r_l (-\Delta H_{rx,l}) \quad 8$$

Boundary conditions for catalyst particles
Symmetry at $r=0$:

$$\frac{\partial C_k^s}{\partial r} = 0 \quad \text{and} \quad \frac{\partial T^s}{\partial r} = 0 \quad 9$$

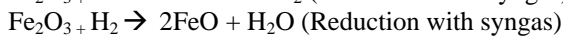
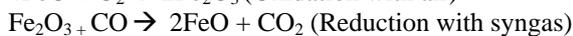
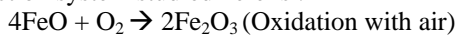
Catalyst surface, $r=R$:

$$\begin{aligned} -\frac{\varepsilon_s D_{eff,k}}{\tau} \frac{\partial C_k^s}{\partial r} &= k_g (C_{k,r=R}^s - C_k) \\ -\lambda \frac{\partial T^s}{\partial r} &= h(T^s - T) \end{aligned} \quad 10$$

For each particle configuration, the 3D CFD-DEM and DEM helps to determine the values of voidage (\mathcal{E}), the Blake–Kozeny–Carman constant (A) and Burke–Plummer constant (B) in Ergun Equation (2), the heat transfer coefficient h and surface area per unit reactor volume a in Equation 6 (see Table 1). The current 1D model uses the reaction kinetics proposed by Abad et. al. (2011) for ilmenite in all the simulations. The 1D model is able to solve for this stiff reactions scheme as it uses an implicit backward differentiation formula for temporal discretization. The upwind scheme is used for the convective terms. The next section provides a brief description of the packed bed reactive CLC process and the validation result.

Chemical looping combustion and validation

The chemical looping combustion packed bed reactors involves cyclic gas-solid non-catalytic reactions, wherein the fixed packing (made of metal/metal oxide particles) is alternatively exposed to fuel gas stream (reduction cycle) and air stream (oxidation cycle). When exposed to the fuel gas stream (syngas), the metal oxide reduces. This reduction cycle results in production of hot stream of carbon dioxide and super-heated steam, which can be used for energy generation. The CO_2 is isolated by condensing steam. The reduced metal oxide bed is then exposed to the air stream, which re-oxidizes it. This exothermic oxidation cycle produces a stream of hot gas that can also be used for energy production. The reduction-oxidation cycle is then repeated continuously leading to power generation and CO_2 capture. The reaction system studied here is:-



In the present validation study, ilmenite ($FeO-Fe_2O_3-TiO_2$) is used as an oxygen carrier. Initially, it is in a fully reduced state (i.e. only $FeO-TiO_2$ is present and no Fe_2O_3 is present). The system is fed with air at inlet temperature of $650^\circ C$ and the initial bed is considered to be at the same temperature. As the oxygen is exposed to the solid ilmenite particle, the exothermic oxidation

reaction takes place. The oxidation reaction continues till the particle is completely oxidized. A reaction front exists as a result of this process. These CLC processes are characterized by the presence of both the reaction front and the thermal front. Both these fronts are identifiable by temperature profile and concentration profile along the reactive bed. The movement of these fronts and the maximum temperature rise predicted by the 1D model is compared to that predicted by an analytical model (Noorman et. al., 2010). The maximum temperature that can be reached in the bed due to the heat liberated by the reaction front and due to the cooling down by incoming gas at the thermal front is obtained using an energy balance, which results in Equation 11. The analytical model provides equation 12 for computing reaction front velocity and Equation 13 for computing thermal front velocity.

$$\Delta T = \frac{(-\Delta H_{Rxn,l})}{\frac{C_{p,s} M_s}{w_{s,j} X_j \tau} - \frac{C_{p,g} M_g}{w_{g,k}^{in}}} \quad 11$$

$$W_r = \frac{\rho_g w_{g,k}^{in} v_g M_{si}}{\varepsilon_s \rho_s w_{s,j} X_j M_{g,k} \xi} \quad 12$$

$$W_h = \frac{\rho_g v_g C_{p,g}}{\varepsilon_s \rho_s C_{p,s}} \quad 13$$

As per the analytical model, the reaction front velocity is 1.12×10^{-2} m/s and the thermal front velocity is 1.43×10^{-3} m/s. The reaction front moves about an order of magnitude faster than the thermal front. Figure 5 shows that the 1D model is able to capture the movement of the reaction front and the thermal front quite accurately. The 1D model shows dispersion in reaction and thermal front as compared to the steep front predicted by analytical model. This dispersion is expected owing to the finite heat transfer rate and finite reaction rate in the actual operation (as is considered in the 1D model). The analytical solution assumes infinite reaction rate and infinite heat transfer rate, which is not a realistic condition. Analytically, predicted maximum temperature rise (equation 11) for the oxidation reaction is about $470^\circ C$. So, the maximum temperature that can be reached in the reactor is about $1120^\circ C$ (Maximum temperature = Inlet air temperature + Max. temperature rise = $650^\circ C + 470^\circ C$).

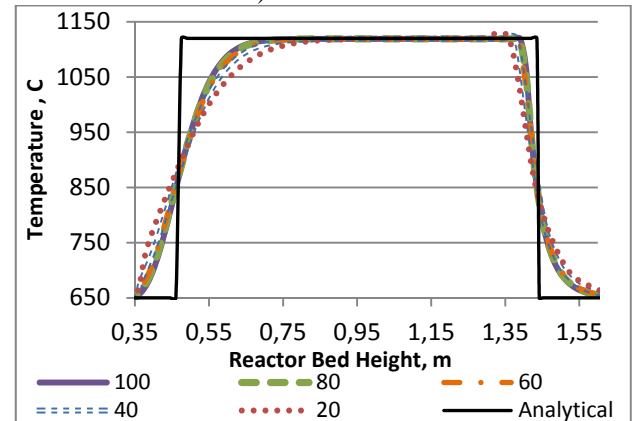


Figure 5 compares 1D model prediction of thermal front movement, reaction front movement and the maximum temperature rise with the analytical result. The results for 1D model are presented at several grid points (20,40,60,80 and 100) to check for grid independence.

Figure 5 shows that the 1D model predicts a maximum temperature of 1120 °C and the bed region between the thermal and reaction front is at this maximum temperature. Thus, the 1D model is able to capture the movement of the thermal and reaction fronts as well as the maximum temperature rise. This validates the use of the 1D model for the non-catalytic gas-solid operations like chemical looping combustion. The validated models have now been used in conjunction to implement the multi-scale approach for reactor design

APPLICATION OF MULTI-SCALE METHODOLOGY FOR OXYGEN CARRIER SELECTION AND CLC REACTOR DESIGN

Figure 6 and 7 compares the performance of seven different particle shape/size configurations for a 500KW fixed bed CLC reactor operation (height 1.5m and diameter 0.3 m) with air fed at 0.81 Kg/s for oxidation and syn-gas fed at for 0.078 Kg/s (corresponding to 500KW inlet heat) for reduction cycle. The comparisons are made for bed conversion, fuel-slip, pressure drop and cycle-time. The closures obtained for different particle configurations by 3D CFD-DEM has been used (See Table 1) by the 1D model. All the 1D simulations have been done using 80 grid points as the solution becomes grid-independent (see Figure 5). The packing configuration that can provide: (a) lower pressure drop, (b) higher reactivity, (c) Zero or minimal fuel-slip, and (c) lower cycle-time operation should be selected for the chemical looping combustion operation.

Table 1 show that some of the particles being studied have the same particle volume (same effective diameter of 7.5mm) but different shapes (sphere-7.5mm, cylindrical pellet with Aspect ratio (AR) of 1, pellet with Aspect ratio of 2 and pellet with Aspect ratio of 7). This will help to understand the effect of shape for a given size.

Particle Shape and size (effective diameter, actual diameter and height)	For Ergun Equation (constants A and B in Equation 2).		For Ranz-Marshall for h in Eqn 6.	Voidage and Surface Area per unit Reactor Volume, m^{-1}
	A	B	A_c	
Sphere (3mm, 5mm and 7.5mm)	150	1.75	1.8	0.4 voidage & 1200 m^{-1} (for 3mm), 780 m^{-1} (for 5mm) and 486 m^{-1} (for 7.5mm).
AR 1 $d_{eff} = 7.5mm$ & $d_{actual} = 6.4mm$, $h_{actual} = 6.4mm$	310	4.56	1.8	0.42 & 538 m^{-1}
AR 2 $d_{eff} = 7.5mm$ & $d_{actual} = 10.26mm$, $h_{actual} = 5.12mm$	180	2	1.8	0.44 & 545 m^{-1}
AR 7 $d_{eff} = 7.5mm$ & $d_{actual} = 3.4mm$, $h_{actual} = 23mm$	210	2.5	1.65	0.545 & 577 m^{-1}
Fluted Ring, AR = 1.4 $d_{eff} = 14mm$ & $d_{actual} = 12.4mm$, $h_{actual} = 17.3mm$	253	2.21	1.68	0.53 & 560 m^{-1}

Table 1. Closures for 1D model from DEM & 3D CFD-DEM.

We also study the effect of size by varying the size for a given spherical shape (3mm, 5mm size and 7.5mm) and a fluted ring with 14 mm effective diameter. All the particles are composed of ilmenite and the reaction kinetics proposed by Abad et. al. (2011) has been used in all the cases. Some of these ilmenite based particle shapes/sizes are being considered for the demonstration scale chemical looping combustion operation at Puertollano, Spain under the EU DemoCLOCK project. This scenario offers an ideal platform for developing and implementing the proposed multi-scale approach using validated models. The results are described below.

For reduction cycle, Figure 6A compares the Fe_2O_3 conversion profile along the length of bed after 60 s of reduction cycle operation for 7 different packing, while Figure 6B shows the overall Fe_2O_3 conversion as a function of time. The reaction front moves the fastest for Aspect ratio 7 packing (Figure 6A) and the whole bed is reduced within 74 s (as seen in Figure 6B). In terms of fastest bed conversion (or fastest reaction front), Aspect ratio 7 is followed by Aspect ratio 2, then the spherical pellets, the Aspect ratio 1 pellet and the Fluted ring. Similar trends are observed for oxidation cycle as well (Figure 7A). These trends are because the voidage of the packing structure increases as pellet aspect ratio increases (as predicted by DEM). Higher voidage results in lower amount of solid mass to be converted in the reactor bed. Figure 3 and Table 1 shows that the DEM predicted voidage for Aspect ratio 7 pellet packing is the highest followed by Aspect ratio 2, followed by spherical particles and Aspect ratio 1. The spherical particle and Aspect ratio 1 pellet shape have more compact packing (less voidage and more mass in the reactor) than the high aspect ratio pellets as a result they need more reactor operation time for complete bed conversion (as seen in Figure 6B-7B and Figure 6A-7A for both the oxidation and reduction). Figure 6A-7A shows that reaction fronts of Aspect ratio 1 and spheres (3mm, 5mm and 7.5mm) move with similar velocity, but have varied dispersions along the similar 'mean' front locations. The dispersion in reaction front increases as the size of sphere increases. The slower the effective reaction rate, higher is the dispersion of the reaction front around the mean location. The reason for this dispersion is the mass-transfer limitations accounted by the particle model of 1D particle-reactor model. As the diameter of sphere increases from 3mm to 7.5mm, the mass-transfer diffusional limitations increases and the effective overall rate of reaction decreases, leading to a more dispersed reaction front for higher diameter spheres. Similarly, the Aspect ratio 1 pellet shows more dispersion in reaction front than Aspect ratio 2 and Aspect ratio 7 pellet. This is because for the same particle volume, the actual diameter of pellets increases with decreasing aspect ratio ($diameter_{AR1} > diameter_{AR2} > diameter_{AR7}$). Thus, the Aspect ratio 1 offers higher mass-transfer diffusional resistance to the reactant gaseous species than Aspect ratio 2 and Aspect ratio 7 pellet.

Now, the Fluted Ring packing also has a higher voidage and very less mass within the reactor (equivalent to Aspect ratio 7 pellet), and even the total particle surface area available is comparable to Aspect ratio 7, so one would expect a quick complete bed conversion

(similar to Aspect ratio 7 case). However, as Figures 6B and 7B reveal that at any given time, the Fluted Ring bed is the least converted amongst all and the bed is not completely converted even after 150 s of reactor operation (only 91% conversion). Figure 6A and 7A reveals that Fluted Ring has the most diffused reaction front amongst all the particles (suggesting a very slow effective rate of reaction). The Fluted Ring has the largest particle diameter amongst all the particles and the mass transfer resistances encountered by the gaseous species would reduce the overall effectiveness. The 1D model is able to capture the mass-transfer limitation within the particle. The mass-transfer limitation dominates the faster intrinsic rate kinetics leading to slower conversion of the fluted ring particle.

Thus, a study of conversion profiles reveal that the Aspect ratio 7 pellet and 3 mm sphere particles offer high reaction rates (owing to lower mass-transfer limitations), while Aspect ratio 7 and Aspect ratio 2 packing results in a faster moving reaction front (owing to higher voidages and lower mass). A study of fuel-slip and pressure drop will enable us to make proper choice.

Figure 6C shows the fuel-slip time for the reduction operation. An early fuel-slip of reactant CO and H₂ will disallow any efficient isolation and capture of CO₂ from the exit-gas stream, thus leading to an unsuccessful operation. An early fuel-slip can occur owing to slower effective reaction rate (i.e. diffused reaction front) caused by mass-transfer limitations. The CO fuel-slip is known to occur earlier than hydrogen fuel slip in all the cases (owing to slow effective rate of reaction of CO). Hence we analyze the CO-slip results to compare the different packed beds. A good packing configuration is where the onset of fuel-slip occurs when nearly most of the bed is converted (i.e. when the reaction front reaches the end). Figure 6C and 6B indicate that the onset time of fuel-slip is better for 3mm sphere (75% bed reduced), followed by Aspect ratio 7 (60% bed reduced), 5mm and 7.5mm spherical particles (nearly 60% reduced), Aspect ratio 2 pellet (40% bed reduced) and Aspect ratio 1 pellet (30% bed reduced). This is expected as the reaction rate is higher for 3mm sphere and the Aspect ratio 7 pellet (as indicated by the sharpness of reaction front) than others. Their high reactivity can be explained on the basis of low diffusional resistances (owing to lower particle diameter) and high particle surface area per unit reactor volume.

Amongst the particle of same volume (i.e. same effective diameter of 7.4 mm but different shape, as shown in Table 1), Aspect ratio 7 provides the highest surface area per unit reactor volume (577 m⁻¹) and the lowest diffusional resistance. For both 3mm sphere and Aspect ratio 7 packed bed, by the time the CO exit gas concentration reaches 5%, almost the entire bed is converted.

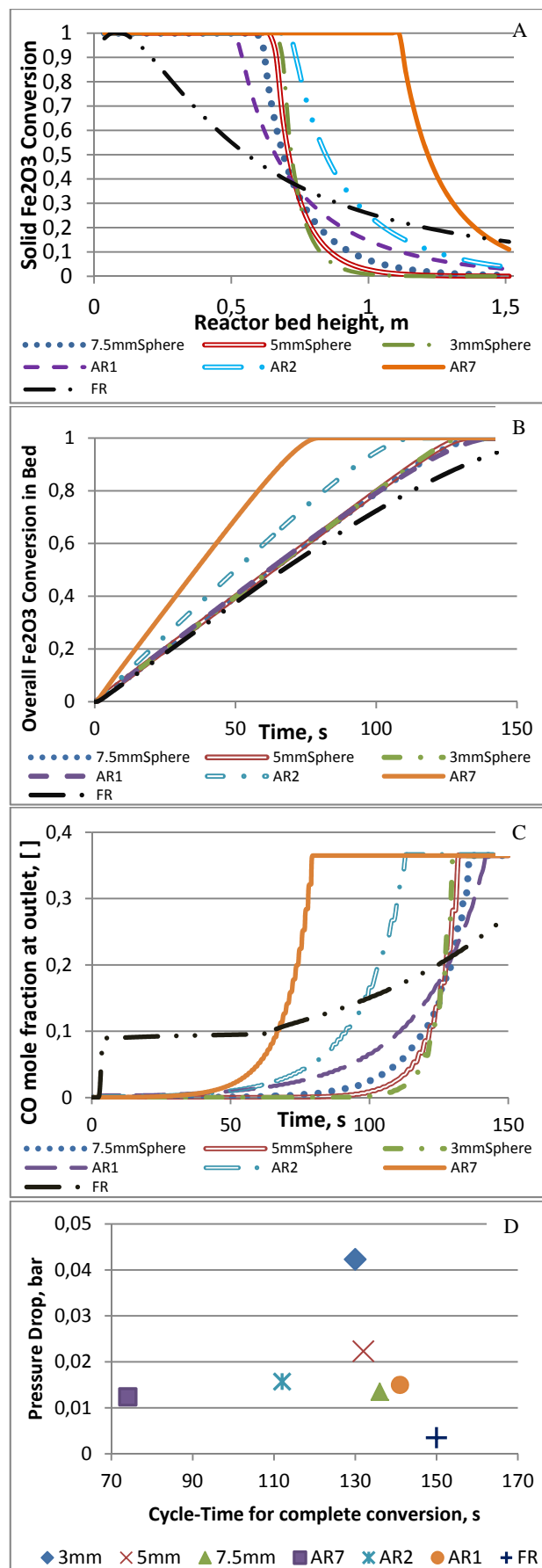


Figure 6 Particle selection for **reduction phase**: comparison of seven different particle configurations : (A) Conversion (Reaction front movement) after 60 s of reactor operation, (B) Overall conversion at a given time, (C) Fuel-slip at reactor exit and (D) Pressure drop and Cycle-time for each particle shape.

With regards to the process, the 14mm Fluted ring can be safely rejected for this CLC application due to a substantial early fuel-slip. This is owing to high mass-transfer limitation that causes a highly diffused reaction front.

Figure 6C and 6B shows that for fluted ring, the fuel slip occurs within first 10 s of reactor start-up and the outlet CO concentration suddenly reaches 10% even though the overall bed is only 5% reduced. Thus, based on the fuel-slip and bed-conversion (reactor bed-utilization) criteria, the Aspect ratio 7 and spherical pellets seem to be good possible choices. However, one needs to look at the pressure drop as well. A higher pressure drop can lower the reaction rate and increase the operating cost. A pressure drop high enough to overcome the weight of the bed can fluidize it or blow it. So, pressure drop is an important criterion.

Figure 6D and 7D shows the pressure drop and cycle-time for packing of each packing configuration for reduction and oxidation, respectively. The figure reveals that the pressure drop is highest for the 3mm sphere followed by 5mm sphere, and is the lowest for the Aspect ratio 7 pellet and fluted ring. The higher particle surface area and lower voidage offered by the 3mm sphere packing ensures that fluid experiences high viscous or skin friction resistance, which results in a higher pressure drop. The pressure drop reduces with increasing sphere size, as is expected. Amongst the particle of same volume, the high voidage in the Aspect ratio 7 packing ensures a lower pressure drop. Though, the pressure drop could have been higher for Aspect ratio 7 and Fluted Ring owing to their higher non-sphericity (which results in higher values of Blake–Kozeny–Carman constant value and the Burke–Plummer constant in the modified Ergun equation, See Table 1) and a higher surface area per unit volume (that can cause higher viscous resistances), but the effect of loose packing (higher voidage) offsets these factors.

From the results of both the oxidation and reduction cycle, it seems that Aspect ratio 7 pellet packed bed can be a good choice as it offers the least pressure drop and high reactivity. In addition, it has a fast moving reaction front that ensures lower cycle-time (thus, lower operating cost) for demonstrating the CLC process. The Aspect ratio 7 pellet performs better than Aspect ratio 2, Aspect ratio 1 and spherical particle of the same particle volume. The alternative can be the 3mm sphere, for which the operating costs could be higher owing to higher pressure drop and higher cycle time (as more mass of catalyst fits in the reactor bed due to low voidage) than the Aspect ratio 7 pellet. However, before finalizing any particle, the ability of the particles to withstand the thermal, chemical and mechanical stress owing to a high temperature-high pressure cyclic operation must be experimentally tested.

Thus, this work has demonstrated the use of a novel multi-scale model in selecting an oxygen carrier for a packed bed chemical looping combustion operation. This methodology can also be applied to create a new catalyst

shape and analyze its performance for a catalytic gas-solid reaction.

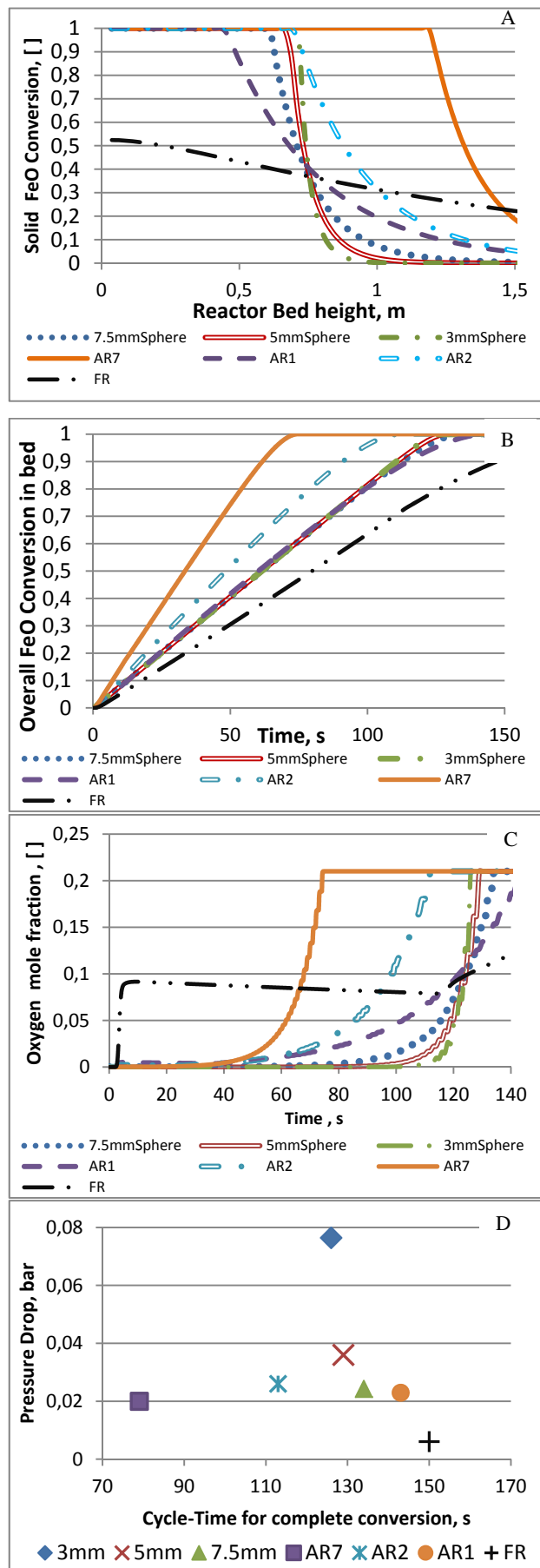


Figure 7 Particle selection for oxidation phase: comparison of seven different particle configurations : (A) Conversion (Reaction front movement) after 60 s of reactor operation, (B)

Overall conversion at a given time, (C) Fuel-slip comparison and (D) Pressure drop and Cycle-time for each particle shape.

CONCLUSION

A multi-scale modelling approach is developed for enabling oxygen carrier selection and reactor design. The approach can potentially be used for catalyst design. The multi-scale approach involves a 3D CFD-DEM (Computational Fluid Dynamics and Discrete Element Method) simulation in-combination with a multi-domain 1D particle-reactor model. In this multi-scale approach, a representative segment of the packed bed (generated by DEM) is simulated using CFD to obtain correlation for pressure drop and heat transfer coefficient. These correlations along with the information on packing structure (i.e. porosity and surface area per unit reactor volume obtained from the DEM generated packing) have been used by the 1D particle-reactor model. The 1D model, which includes the inter-particle and intra-particle limitations, is used for simulating the large scale packed bed reactor. The multi-scale approach provides a faster and reasonably accurate means of comparing the effect of oxygen carrier (or catalyst or pellet shape) on reactor performance.

The multi-scale model has been applied to compare performance of different particle configurations (spherical, Aspect ratio 7 pellet, Aspect ratio 2 pellet, Aspect ratio 1 pellet and fluted ring) for a gas-solid non-catalytic chemical looping combustion packed bed reactor. For particles of same equivalent diameter (volume), the Aspect ratio 7 pellet filled reactor offers the least pressure drop, highest reactivity and provides a lower cycle-time operation as compared to spherical pellets and other low aspect ratio cylindrical pellets. The higher voidage created by the aspect ratio 7 packing is the reason for the lower pressure drop. Further, the high surface area per unit reactor volume and lower actual pellet diameter (low diffusional resistance) of aspect ratio 7 packing leads to high catalyst effectiveness, faster reaction rates and avoids early fuel-slip. The 14mm fluted ring offers higher diffusional limitations that results in slower reaction rates and early CO fuel slip is rejected as it will prohibit the isolation and capture of CO₂.

Thus, the work has successfully demonstrated a novel multi-scale modeling approach involving 3D-DEM-CFD-1D model for selecting optimum size/shape of pellets for a packed bed reactor operation. This methodology can be applied to create new particle shapes and analyze their performance (for catalyst design) and for studying pre-existing shapes (like tri-lobe quadrulobe, monoliths, wagon wheels, hollow extrudates, discs etc.).

ACKNOWLEDGEMENT

A POP-SEP funding from SINTEF has been used for the 1D particle-reactor model software development. The multi-scale model development has been carried out as a part of the DemoCLOCK project, which is an EU FP7 funded project under the ENERGY.2010.6.1-1 programme.

REFERENCES

- ABAD, A., ADÁNEZ, J., CUADRAT, A., GARCÍA-LABIANO, F., GAYÁN, P., AND DE DIEGO, L. F. (2011), "Kinetics of redox reactions of ilmenite for chemical-looping combustion", *Chemical Engineering Science*, **66**, 92-97.
- BEY, O., AND EIGENBERGER, G., (1997) , "Fluid flow through catalyst filled tubes", *Chem Eng Sci*, **52**, 1365-1376.
- CAULKIN, R., JIA, X., FAIRWEATHER, AND M. WILLIAMS, R.A., (2012), "Predictions of porosity and fluid distribution through nonspherical-packed columns", *AIChE Journal*, **58**, 1503-1512.
- COLLEDGE, R.A.P. AND PATTERSON, W. R., (1984) , "Heat Transfer at the Wall of a Packed Bed: A j-Factor Analogy established", *11th Annual Research Meeting; Institution of Chemical Engineers: Bath*, 6 .
- DIXON, A.G. AND LABUA, L.A., (1985), Wall-to-fluid coefficients for fixed bed heat and mass transfer, *International Journal of Heat and Mass Transfer*, **28**, 879-881.
- DIXON, A.G., (1988), Correlations for wall and particle shape effects on fixed bed bulk voidage, *Canadian Journal of Chemical Engineering*, **66**, 705-708.
- DEKLERK, (2003) "Voidage variation in packed beds at small column to particle diameter ratio", *AIChE Journal*, **49**, 2022-2029.
- ERGUN, S., Fluid Flow through Packed Columns, *Chem. Eng. Prog.*, **48** (1952) 89.
- GIESE, M., ROTTSCHÄFER, K., AND VORTMEYER, D., (1998), "Measured and Modeled Superficial Flow Profiles in Packed Beds with Liquid Flow", *AIChE Journal*, **44** , 484-490.
- INGRAM, G.D., CAMERON, I.T., AND HANGOS K.M., (2004), "Classification and analysis of integrating frameworks in multiscale modelling", *Chem Eng Sci*, **59** 2171-2187.
- NEMEC, D. AND LEVEC, J., (2005), "Flow through packed bed reactors: 1. Single-phase flow", *Chem Eng Sci*, **60** , 6947-6957.
- NOORMAN, S., VAN SINT ANNALAND, M., AND KUIPERS, J. A. M, (2010), "Experimental validation of packed bed chemical-looping combustion", *Chemical Engineering Science*, **50**, 1968-1980.
- RANZ, W.E. AND MARSHALL, (1952), W.R. "Evaporation from Drops, Part II.", *Chem. Eng. Prog.* , **48**, 173.
- ROBLEE, L.H.S., BAIRD, R. M. AND TIERNEY, J. W., (1958) , "Radial porosity variations in packed beds", *A.I.Ch.E.J.*, 460-464.
- TABIB, M.V., JOHANSEN, S.T., AND SHAHRIAR, A., (2013), "A 3D CFD-DEM methodology for simulating industrial scale packed bed Chemical Looping Combustion reactors", *Industrial and Engineering Chemistry Research*, **52** (34) 12041–12058.
- WAKAO, N., KAGUEI, S., AND FUNAZKRI, T. (1979), "Effect of fluid dispersion coefficients on particle-to-fluid heat transfer coefficients in packed beds: Correlation of nusselt numbers", *Chem. Eng. Sci.*, **34**, 325–336.